

# Essentially Optimal Explicit Runge-Kutta Methods with Application to Hyperbolic-Parabolic Equations

Manuel Torrilhon and Rolf Jeltsch

Research Report No. 2008-21  
May 2008

Seminar für Angewandte Mathematik  
Eidgenössische Technische Hochschule  
CH-8092 Zürich  
Switzerland

# Essentially Optimal Explicit Runge-Kutta Methods with Application to Hyperbolic-Parabolic Equations

Manuel Torrilhon and Rolf Jeltsch

Seminar für Angewandte Mathematik  
Eidgenössische Technische Hochschule  
CH-8092 Zürich  
Switzerland

Research Report No. 2008-21

May 2008

## Abstract

Optimal explicit Runge-Kutta methods consider more stages in order to include a particular spectrum in their stability domain and thus reduce time step restrictions. This idea, so far used mostly for real line spectra, is generalized to more general spectra in the form of a thin region. In thin regions the eigenvalues may extend away from the real axis into the imaginary plane. We give a direct characterization of optimal stability polynomials containing a maximal thin region and calculate these polynomials for various cases. Semi-discretizations of hyperbolic-parabolic equations are a relevant application which exhibit a thin region spectrum. As a model, linear, scalar advection-diffusion is investigated. The second order stabilized explicit Runge-Kutta methods derived from the stability polynomials are applied to advection-diffusion and compressible, viscous fluid dynamics in numerical experiments. Due to the stabilization the time step can be controlled solely from the hyperbolic CFL condition even in the presence of viscous fluxes.

# 1 Introduction

Time integration methods for ordinary differential equations are classified into implicit and explicit methods. In implicit methods a possibly large and non-linear system of equations is needed to be solved in each time step which makes those methods computationally expensive and difficult to implement. On the other hand, explicit methods require only function evaluations of the right hand side of the ODE. However, explicit methods are subject to time step conditions, which are much more restrictive than those for implicit methods. An extensive introduction, investigation and discussion of numerical methods for ODEs can be found in the text books [4] by Hairer, Norsett and Wanner and [5] by Hairer and Wanner.

An interesting approach to combine both implicit and explicit methods stabilizes the explicit methods by increasing the number of internal explicit stages. An overview over these stabilized method and detailed references can be found in [5], and [7]. The stages are chosen such that the stability condition of the explicit method is improved. In many cases the stabilized methods exhibit similar efficiencies as implicit methods. Additionally, they are very easy to implement.

The theoretical paradigm of stabilized explicit methods is the following: For a given spectrum of an ODE, find a stability domain that includes this spectrum with an optimal number of explicit stages. So far, stabilized explicit methods have been mainly develop with increased stability domain along the real axis. This case applies to parabolic equations where the spectrum is given by an interval of the negative real line. Lebedev in [11] and Lebedev and Medovikov in [12] developed higher order optimal stability polynomial for a maximal real interval. A third order method is described in [14] by Medovikov. The paper [6] by van der Houwen and Sommeijer describes an approach based on orthogonal polynomials which was implemented and used in [17] by Sommeijer, Shampine and Verwer. Abdulle and Medovikov in [1] combined both approaches and Abdulle extended it to higher order in [2].

This paper provides a theory to derive essentially optimal explicit stability domains for more general spectra, that go beyond the classical case of a real interval. We consider spectra in the shape of *thin regions* placed along the real line but also extending slightly into the imaginary plane. The thin region can have very general shape, as long as a high aspect ratio between real and imaginary extension is maintained. We present a working hypothesis about a general characterization of the optimal stability domain for thin regions. The application of our characterization proved to be useful in the approximate construction of stability domains which may be considered as essentially optimal. In our algorithm the calculation of an optimal stability polynomial requires only the solution of a non-linear system. Several optimal stability domains for various thin regions are presented.

Recently, in [20], Verwer, Sommeijer and Hundsdorfer apply Runge-Kutta-Chebyshev methods to advection-diffusion problems. They use damping strategies to fit ellipses and ovals into the stability domain. The approach of the present paper is more general and allows to optimize the stability domain for a wider class of shapes. A comparison of the new approach to stability domains obtained by damping is shown at the end of Sec. 3.

In the second part of this paper we will consider semi-discretizations of hyperbolic-parabolic equations as an example where a thin region spectrum occurs in applications. The applications we have in mind are instationary simulations of compressible, viscous gas dynamics. The equations are built from the hyperbolic inviscid first order system supplemented with a dissipative, parabolic second order operator representing viscosity and heat conduction. As soon as a hyperbolic flux is simultaneously discretized with a parabolic operator, the semi-discrete system shows a spectrum not any more confined on the real line. Instead, the spectrum exhibits the shape of a thin region. In principle, both spatial operators in a hyperbolic-parabolic equation could be discretized and solved separately in a splitting approach. However, splitting is considered to miss the physical reality and to introduce additional error sources. Hence, a fully coupled

numerical discretization will be considered in this paper.

The optimal stability domains and corresponding Runge-Kutta methods are developed on the basis of scalar advection-diffusion and then applied to the system of gas dynamics. Purely hyperbolic systems are almost always solved by explicit methods and stability requires only  $\Delta t \sim \Delta x$  for the time step. However, when viscous gradients are added the system is stiffened and the time step conditions becomes more restrictive for large viscosity or fine grids. The stabilized explicit methods derived in this paper will allow to keep a hyperbolic time step even with viscous terms in an efficient and easy way.

The first part of the paper will present and discuss the theory of optimal stability domains for thin regions. In Sec. 2 we introduce the notion of optimality for explicit Runge-Kutta methods. Thin regions are defined in Sec. 3 and the theory of thin region stability is developed. A direct characterization in form of an explicit system of nonlinear equations describes optimal stability domains for thin regions. Examples of optimal thin region stability domains are presented at the end of Sec. 3. The second part of the paper applies the theoretical results to advection-diffusion and gas dynamics. Sec. 4 introduces semi-discrete finite-volume methods for hyperbolic-parabolic equations. As an appropriate model the semi-discrete advection-diffusion equation is introduced and its eigenvalue structure identified as thin region. In Sec. 5 optimal stability domains and corresponding Runge-Kutta methods are derived for this case. Sec. 6 presents numerical experiments for both the advection-diffusion equation and compressible, viscous fluid dynamics in one space dimension.

The example code for the advection-diffusion equation together with the data of the optimized stability polynomials are available online through [18].

## 2 Optimal explicit Runge-Kutta methods

We will consider explicit Runge-Kutta methods for the numerical solution of an ordinary differential equation

$$y'(t) = F(y(t)) \quad (1)$$

with  $y : \mathbb{R}^+ \rightarrow V \subset \mathbb{R}^N$  and  $y(0) = y_0$ . An extensive presentation and investigation of Runge-Kutta methods can be found in the textbooks [4] and [5]. The stability function of a  $p$ -th order,  $s$ -stage explicit Runge-Kutta method is a polynomial in the form

$$f_s(z) = 1 + \sum_{k=1}^p \frac{z^k}{k!} + \sum_{k=p+1}^s \alpha_k z^k \quad (2)$$

with  $p \leq s$ . We call  $p$  the order of  $f_s(z)$ . The stability domain of the method is given by

$$S(f_s) = \{z \in \mathbb{C} \mid |f_s(z)| \leq 1\}. \quad (3)$$

If the method is applied to the ordinary differential equation (1) with a certain time step  $\Delta t$ , the set of the scaled eigenvalues of the Jacobian of  $F$  with negative real part

$$G^{(\Delta t)} = \{\Delta t \lambda \in \mathbb{C} \mid \lambda \text{ eigenvalue of } DF(y), \operatorname{Re} \lambda \leq 0, y \in V\} \quad (4)$$

has to be included the stability domain of the method in order to assure stability. This is referred to as linear stability of the method.

Suppose the order  $p$  of the method is fixed, then for  $s > p$  the remaining coefficients of the stability polynomial (2) can be viewed as parameters which control the shape of the stability domain. For a given equation (1) and time step  $\Delta t$  the problem of an optimal explicit method can be formulated as:

$$\text{Find } \{\alpha_k\}_{k=p+1}^s \text{ for minimal } s, \text{ such that } G^{(\Delta t)} \subset S(f_s). \quad (5)$$

The coefficients are used to adapt the stability domain to a fixed set of eigenvalues of  $DF$ . In many cases the set of eigenvalues changes shape according to a real parameter  $r \in \mathbb{R}$  which is not necessarily the time step. For example, the value  $r$  could be the length of a real interval or the radius of a disk. This paper considers a family of eigenvalue sets given by  $G_r \subset \mathbb{C}$ ,  $r \in \mathbb{R}_+$ . We consider the following optimization problem:

**Problem 1** For fixed  $s$  and  $p$  find  $\{\alpha_k\}_{k=p+1}^s$  for the largest  $r$  such that

$$G_r \subset S(f_s) \quad (6)$$

and  $f_s(z)$  given by (2).

Here, the number of stages as well as the order is fixed and both the shape of  $G_r$  and the coefficients of the stability polynomial are adapted to each other in order to obtain the maximal value of  $r$ . The maximal  $r$  is called  $r_p^{(opt)}(s)$ , that is

$$r_p^{(opt)}(s) = \max \{r \in \mathbb{R} \mid G_r \subset S(f_s), p \text{ order of } f_s\}. \quad (7)$$

In all families of  $G_r$  which we considered there existed an optimal  $f_s$ . It is clear that the result of this optimization of  $r$  is related to the optimization (5). The inversion of the relation  $r_p^{(opt)}(s)$  which gives the maximal value of  $r$  for a number of stages  $s$  can be used to find the minimal number of stages for a given value of  $r$ .

Specific cases of  $G_r$  are covered by classical results. The case of a disk is studied in [10] and [9] for first order polynomials and in [16] for higher order. Roughly, an  $s$ -stage,  $p$ -th order Runge-Kutta method can be built such that a disk with radius  $r = s - p + 1$  is included in the stability domain. The case of a real interval  $[-r, 0]$  is interesting for parabolic equations. The first order polynomials are given by shifted Chebyshev polynomials which allow  $r = 2s^2$ . Higher order has been considered by various authors, see the discussion in the Introduction. A second order optimal polynomial for the real interval is shown in Fig. 4.

### 3 Essentially optimal thin region stability

In this section we consider regions  $G_r$  which are to some extent a combination of disks and real intervals. We note that this is necessary in applications like compressible, viscous flow problems. The generalized regions  $G_r$  are called *thin regions*.

#### 3.1 Thin regions

As all stability regions are symmetric with respect to the real axis, we shall assume the same for a thin region. The two main parameters of a thin region are  $r$  which is given by the largest interval  $[-r, 0]$  contained in  $G_r$  and  $\delta$  which is  $\max(\text{Im } z \mid z \in G_r)$ . We shall develop in this section a technique to determine optimal stability domains for a given family of thin regions  $G_r$ 's. The technique is relying on the properties of the optimal stability result for the real interval, and hence we mean by thin that  $\delta \ll r$ .

The following definition assumes that a thin region is symmetric and is generated by a continuous real function.

**Definition 1 (thin region)** The region  $G_r \subset \mathbb{C}$  is called a thin region, if there exists a positive, real continuous function  $g_r(x)$ ,  $x \in [-r, 0]$  with  $g_r(0) = g_r(-r) = 0$ ,  $\max_{x \in [-r, 0]} g_r(x) = \delta$  and  $r > 0$  such that

$$G_r = \{z \in \mathbb{C} \mid |\text{Im } z| \leq g_r(\text{Re } z), \text{Re } z \in [-r, 0]\} \quad (8)$$

and  $\delta/r \ll 1$ .

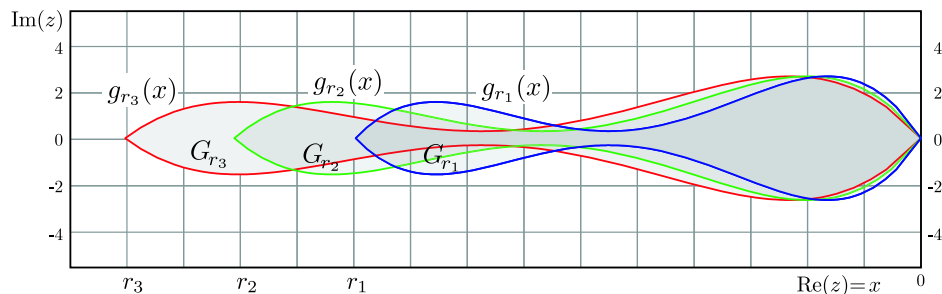


**Figure 1:** Example of thin regions  $G_r$  spanned by  $g_r(x)$  for different values of  $r$ . In general  $G_r$  may have different shapes for different values of  $r$ .

The case  $g_r \equiv 0$  produces the real interval as degenerated thin region. If a continuous function  $\hat{g} : [-1, 0] \rightarrow [0, 1]$  is given, the thin region constructed by  $g_r(a) = \delta \hat{g}(\frac{a}{r})$  is an affine mapping of  $\hat{g}$  with  $\hat{g}(-1) = \hat{g}(0) = 0$ . For example  $\hat{g}(x) = \sqrt{-x(1+x)}$  leads to a stretched ellipse with halfaxes  $r$  and  $\delta$ . A more complicated case is displayed for different values of  $r$  in Fig. 1. In Sec. 3.5 more examples will be given. In the definition  $g_r$  is generally parametrized by  $r$ . Hence, a family of thin regions  $\{G_r\}_{r \in \mathbb{R}}$  may exhibit a different shape for different values of  $r$  not only a shape obtained by affine mappings. However, the maximal thickness  $\delta$  shall remain the same for all values of  $r$ .

The real axis extension  $r$  of a thin region will be our main parameter. In the following we will investigate how to derive optimal stability domains in the sense of (6) for thin regions. The stages will be optimized such that the stability domain allows a thin region  $G_r$  with maximal  $r$ . We will speak of a *maximal* thin region which refers to a maximal extension  $r$  along the real axis at a given value of  $\delta$ . A stability polynomial  $f_s$  with given order  $p$  and stages  $s$  that includes a maximal thin region in its stability domain will be called *optimal* for this thin region.

Later we will give a concrete example of ordinary differential equations in which the eigenvalues of the Jacobian form a thin region, namely semi-discretizations of advection-diffusion equations.

### 3.2 Working Hypothesis

From the classical results for stability domains with maximal real interval and maximal disks, we suspect that the boundary of the optimal stability domain touches the boundary of  $G_r$  at  $s - p$  positions in the upper half plane. In addition from the maximal real interval case we note that these places of touching are related to the extrema of  $f_s$  along the real axis which are close to  $\pm 1$ . Our working hypothesis is that controlling these extrema is essential to characterize and calculate the optimal stability domains of thin regions. See the results for the examples in Sec. 3.5, which help to develop an intuition for this approach.

**Working-Hypothesis 1 (maximal thin region stability)** *Let  $f_s$  be the optimal stability polynomial with order  $p \in \{1, 2\}$  for a thin region  $G_r$  given by a  $g_r \in C^2$  which is positive for all  $\text{Re } z \in (-r, 0)$  with thickness  $\delta > 0$  and  $\delta/r \ll 1$ . Then we have*

i)  $f_s(-r) \leq 1$

ii) *the boundary of the optimal stability domain of  $f_s$  touches in a smooth way the boundary of the thin region in  $(-r, 0) \times (0, \delta]$*

- *in  $s - p$  points, if ' $\leq$ ' holds in i),*
- *in  $s - p + 1$  points, if '<' holds in i)*

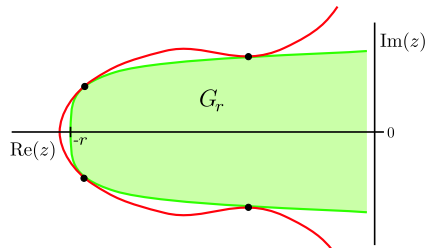


**Figure 2:** Sketch of the case ' $<$ ' in i) of the working hypothesis. The opening angle of  $G_r$  is too large, so that two additional touching points are produced to allow an maximal value of  $r$ .

and the real parts of these touching points are located in the vicinity of the extremal points of  $f_s$  along the negative real line.

By touching smoothly we mean, that both curves are differentiable and have the same tangents.

**Remark 1** In all our practical examples this working hypothesis led to an essentially optimal real extension  $r$ .

**Remark 2** Condition i) is obvious. In condition ii) it is clear, that if the boundary of  $G_r$  and the boundary of the stability region  $S(f_s)$  have a common point in  $(-r, 0) \times (0, \delta]$  then the tangents to the boundaries can not cross. There is an obvious relation between condition i) and ii). If ' $<$ ' holds in condition i) then there is an additional touching of the two boundaries. See Fig. 2 for a sketch of the situation. If ' $=$ ' holds in condition i) this additional touching of the two boundaries has in fact moved to the point  $-r$ . The case ' $=$ ' in condition i) can be assumed if  $g_r$  satisfy certain conditions in the vicinity of  $-r$ . To be precise, the opening angle of  $g_r$  at  $-r$  has to be included in the opening of the stability domain which can be checked by asymptotic analysis, see below.

**Remark 3** The statement of the relative position of real parts of the touching points and the extrema of  $f_s$  along the negative real line is in a sense vague. Hence a rigorous proof of this working hypothesis would need a more precise specification. Nevertheless, the exploitation of this hypothesis leads to useful practical results in the following.

In the case of a real interval  $G_r = [-r, 0]$  the assertion is true. However, at the points where the boundary of  $G_r$  and the boundary of the stability region  $S(f_s)$  have a common point, only one sided tangents to the boundary of the stability region  $S(f_s)$  exist and in fact these tangents are not equal to the one of the boundary of  $G_r$ . In this situation the touching points are turned into what one might call a kink. This is due to the fact that  $G_r$  has now interior points. To avoid this situation we look only at cases where  $g_r$  is strictly positive in  $(-r, 0)$ . In the maximal real interval case, for  $p = 1$  all  $s - 1$  extrema have values of  $\pm 1$  and produce boundary points which lie on the real axis. For  $p = 2$  one extrema is fixed by the order conditions, but  $s - 2$  extrema at  $\pm 1$  again produce kinks in the boundary that touch the real axis. For small aspect ratio  $\delta/r$  a thin region can be viewed as a perturbation of the domain given by a real interval alone. If any of the extrema is lowered away from  $\pm 1$ , the kinks of the boundary are lifted and form dented curves which release some margin for a thin region. Necessarily, the maximally included real interval would be shortened. The minimums in these curves replace the kinks and will be referred to as denting points. Intuitively, a maximized real extension of the stability domain is realized only if all the denting points are as close to the real axis as possible. Hence, they have to touch the boundary of the thin region.

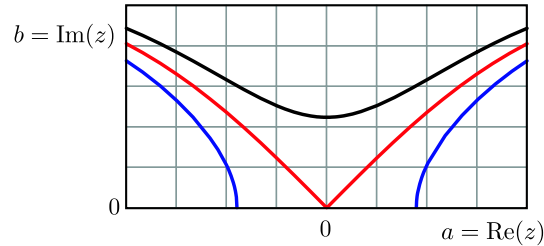


**Figure 3:** Behavior of the boundary of the stability domain in the vicinity of a real extremum close to unity. The shape changes according to value and curvature of the extremum.

Existence and uniqueness of the optimal thin region stability polynomial is viewed in this perturbation setting. For the case of a real interval appropriate results are given in various papers. If the polynomial deviates only little from this limiting case in the way described by the working hypothesis, we expect these results still to be valid. However, a rigorous proof is left for future work.

Instead we will study the behavior of the denting points and give two examples in which everything can be calculated explicitly, in order to support the working hypothesis.

The denting points in the boundary are formed by the real extrema of  $f_s$ . To understand their behavior we consider

$$h(z) = \alpha + \beta z^2 \quad (9)$$

with  $\alpha, \beta \in \mathbb{R}$  as an approximation of  $f_s$  around a generic extrema at  $z = 0$ . We consider  $z = a + b(a)\mathbf{i}$  with  $a \in \mathbb{R}$ . The function  $b(a)$  is implicitly given by the boundary condition  $|h(a + b(a)\mathbf{i})| = 1$  and has the form

$$b(a) = \pm \sqrt{\frac{\alpha}{\beta} - a^2 + \frac{\text{sign}(\beta)}{\beta} \sqrt{1 - 4\alpha\beta a^2}} \quad (10)$$

of which we will only consider the positive part. The behavior of this function is depicted in Fig. 3 for  $\alpha = 0.9, 1.0, 1.1$  and  $\beta = 0.25$ . The point  $a = 0$  with  $b(0) = \pm \sqrt{(\alpha + \text{sign}(\beta))/\beta}$  corresponds to the extremal point of  $h(z)$  at  $z = 0$ . For  $\alpha = -\text{sign}(\beta) \in \{\pm 1\}$  we have either a maximum with value 1 or a minimum with value  $-1$ . Both cases yield  $b(0) = 0$  and  $b''(0) \rightarrow \infty$ , hence, a kink which touches the real axis. For  $\alpha \text{sign}(\beta) < -1$  the maximum of  $h(z)$  reaches values  $> 1$  or the minimum values  $< -1$ . It follows  $b(0) \in \mathbb{C}$  and the stability domain is split into two parts at this extremum. Both cases are shown in Fig. 3. In the case  $\alpha \text{sign}(\beta) > -1$  the boundary  $b(a)$  exhibits a minimum which leaves a margin of  $\sqrt{(\alpha + \text{sign}(\beta))/\beta}$  between the boundary and the real axis.

The position of the denting points is roughly described by the position, value and curvature of the extrema of  $f_s$ . Of course, the position of the extrema will in turn influence the real extension of the stability domain. The working hypothesis states that for a given optimal stability polynomial for a thin region the lifting of any denting point will result in a reduction of the real extension.

To prove this, one would need to find a general monotone relation of the position of a single denting point in the boundary with the real extension of the stability domain at least for small values of  $\delta$ . In the following examples we will consider simplified situations. Both examples consider the first order case. The first example deals with  $s = 2$  and only one denting point is there to be controlled. The second case allows arbitrary  $s$  but the all denting points are controlled simultaneously along an ellipse. In both cases we find a monotone relation between the margin opened by the denting points and the real extension  $r(\delta)$ .

**Example 1 (two-stage, first order)** For  $r \in \mathbb{R}$  and  $0 < r \leq 8$  the stability polynomial

$$f(z) = 1 + z + \frac{1}{r}z^2 \quad (11)$$

has a stability domain which includes the real interval  $[-r, 0]$ . The stability domain is convex for  $2 \leq r \leq 6$ . For  $6 < r < 8$  two symmetric denting points in the boundary of the stability domain appears at  $z_D = r/2 \pm \mathbf{i}\delta(r)$  with

$$\delta(r) = \frac{1}{2}\sqrt{r(8-r)}, \quad r(\delta) = 4(1 + \sqrt{1 - \delta^2/4}) \quad (12)$$

for the distance between the boundary and the real axis. Obviously,  $r(\delta)$  is monotonically decreasing with increasing  $\delta$  in the interval  $[0, 2]$ . At  $\delta = 0$  and  $r = 8$  the denting points hit the real axis as a sharp edge and  $f(z)$  turns into the shifted Chebyshev polynomial. For  $r > 8$  the stability domain breaks apart into two distinct regions.

Due to the denting point the stability domain has a barbell-like shape and the available margin around the real axis shrinks as  $r$  grows. If a thin region requires at least a margin of  $\tilde{\delta} < 1$  only the choice of  $r(\tilde{\delta})$  will result in a maximal extension along the real axis. Hence, the denting points touch the boundary of the thin region.

The second example considers a disturbance of the optimal polynomials for the real interval given by Chebyshev polynomials, see also [19] and [20] for related cases.

**Example 2 (damped Chebyshev polynomials)** The stability polynomials

$$f_s(z) = (1 - \varepsilon) T_s \left( \frac{x + \Delta x_\varepsilon}{\theta_\varepsilon s^2} + 1 \right) \quad (13)$$

with  $s \geq 2$  are built from Chebyshev polynomials. They resemble the case of the optimal polynomials for a real interval, but are damped by  $1 - \varepsilon$  ( $\varepsilon \geq 0$ ) and additionally shifted and stretched by  $\Delta x_\varepsilon$  and  $\theta_\varepsilon$ . These two parameters follow depending on  $\varepsilon$  from the order conditions  $f_s(0) = f'_s(0) = 1$  and we find  $\theta_\varepsilon = 1 - \frac{2s^2+1}{3s^2}\varepsilon + \mathcal{O}(\varepsilon^2)$  and  $\Delta x_\varepsilon = \varepsilon + \mathcal{O}(\varepsilon^2)$ . The extrema of the polynomial along the real line are given by

$$x_E^{(k)} = \frac{r_\varepsilon}{2} \left( \cos \left( \frac{k\pi}{s} \right) - 1 \right), \quad k = 1, 2, \dots, s-1. \quad (14)$$

At these extremal points the boundary of the stability domain has denting points which reach the real axis at  $\varepsilon = 0$  but open some margin of size  $\delta_E^{(k)}$  for  $\varepsilon > 0$ . With (10) for  $a = 0$  we find

$$\delta_E^{(k)} = \sqrt{\frac{1 - f_s(x_E^{(k)}) \operatorname{sign}(f_s''(x_E^{(k)}))}{\frac{1}{2} |f_s''(x_E^{(k)})|}} = s \theta_\varepsilon \sqrt{\frac{2\varepsilon}{1 - \varepsilon}} \sin \left( \frac{k\pi}{s} \right), \quad (15)$$

hence the denting points of the boundary are located along the ellipse  $z_D^{(k)} = \frac{r_\varepsilon}{2} \left( \cos \left( \frac{k\pi}{s} \right) - 1 \right) \pm \mathbf{i} \delta_\varepsilon \sin \left( \frac{k\pi}{s} \right)$  with

$$\delta_\varepsilon = s \theta_\varepsilon \sqrt{\frac{2\varepsilon}{1 - \varepsilon}} = s\sqrt{2\varepsilon} + \mathcal{O}(\varepsilon^{3/2}) \quad (16)$$

for the width of the ellipse. The maximal included real interval is given by

$$r_\varepsilon = 2s^2 \left( \theta_\varepsilon + \frac{\Delta x_\varepsilon}{s^2} \right) = 2s^2 \left( 1 - \frac{2s^2+1}{3s^2}\varepsilon \right) + \mathcal{O}(\varepsilon^2) \quad (17)$$

which can be written in terms of  $\delta_\varepsilon$

$$\frac{r(\delta_\varepsilon)}{2s^2} = 1 - \frac{1}{3} \frac{s^2-1}{s^4} \delta_\varepsilon^2. \quad (18)$$

The scaled length of the included real interval is monotonically shortened with increasing margin  $\delta_\varepsilon$  of the ellipse.

We conclude that the denting points of the stability domain of damped Chebyshev polynomials can be controlled in form of an ellipse. A thin region in the form of an ellipse with given thickness  $\tilde{\delta} < 1$  would fit in the stability domain for any  $\varepsilon$  such that  $\delta_\varepsilon \geq \tilde{\delta}$ , but only for  $\delta_\varepsilon = \tilde{\delta}$  we obtain the maximal real extension  $r(\tilde{\delta})$ . In that case the denting points of the stability boundary touch the boundary of the ellipse. The optimality can also be viewed as inherited from the optimality of the Chebyshev polynomials, since, even with a fixed damping parameter we obtain a maximal real line extension.

### 3.3 Characterization

For second order and general shapes of thin regions we leave the claim of the working hypothesis open. Nevertheless, we trust the statement and use it to characterize and calculate optimal stability polynomials for thin regions. The results are demonstrated to be useful in the next sections. We will mainly consider second order polynomials.

**Proposition 1 (extrema characterization)** *Let  $r > 0$  and  $G_r \subset \mathbb{C}$  be a convex thin region in  $[-r, 0] \times [-\delta, \delta]$  with a sufficiently small aspect ratio  $\delta/r$  described by a function  $g_r \in C^2(-r, 0)$ . We assume that there exists an optimal stability polynomial and that the working hypothesis is correct with '=' in condition i). Let  $f_s(z)$  be this optimal second order stability polynomial whose stability domain  $S(f_s) \subset \mathbb{C}$  contains  $G_r$  with maximal value for  $r$ . For  $x \in \mathbb{R}$  the function  $f_s(x)$  has  $s-1$  extrema at the points  $-r < x_1 < x_2 < \dots < x_{s-1} < 0$ . Let  $\varepsilon = \max_{k=1}^{s-2} \{f_s'''(x_k), (g_r'(x_k))^2\}$ . Then the first  $s-2$  extrema are satisfying*

$$g_r(x_k) = \sqrt{\frac{1 + f_s(x_k) \operatorname{sign}(f_s''(x_k))}{\frac{1}{2} |f_s''(x_k)|}} \left( 1 + \frac{g_r'(x_k)^2}{2(1 + 2f_s(x_k) \operatorname{sign}(f_s''(x_k)))} \right) + \mathcal{O}(\varepsilon) \quad (19)$$

with  $k = 1, 2, \dots, s-2$  and, furthermore, the points  $\hat{z}_k = \hat{x}_k + g_r(\hat{x}_k) \mathbf{i}$  with

$$\hat{x}_k = x_k - \frac{g_r'(x_k)}{(1 + 2f_s(x_k) \operatorname{sign}(f_s''(x_k)))} \sqrt{\frac{1 + f_s(x_k) \operatorname{sign}(f_s''(x_k))}{\frac{1}{2} |f_s''(x_k)|}} + \mathcal{O}(\varepsilon) \quad (20)$$

are boundary points of  $S(f_s)$ .

**Proof.** The relation (10) describes the boundary behavior  $b_k(a)$ , in the vicinity of each extrema  $x_k$ ,  $k = 1, 2, \dots, s-2$  of the function  $f_s$  up to an error  $\mathcal{O}(f_s'''(x_k))$  with the values  $\alpha = f_s(x_k)$ ,  $\beta = \frac{1}{2} f_s''(x_k)$  and  $a = x - x_k$ . We consider the Taylor expansion for  $|x - x_k| \ll 1$  and obtain

$$b_k(x) = \sqrt{\frac{1 + f_s(x_k) \operatorname{sign}(f_s''(x_k))}{\frac{1}{2} |f_s''(x_k)|}} \left( 1 - \frac{|f_s''(x_k)| (1 + 2f_s(x_k) \operatorname{sign}(f_s''(x_k)))}{4(1 + f_s(x_k) \operatorname{sign}(f_s''(x_k)))} (x - x_k)^2 \right) + \mathcal{O}((x - x_k)^3). \quad (21)$$

Since the extrema are the points at which the boundary is closest to the real axis, an optimal stability polynomial will touch the boundary of the thin region  $g_r(x)$  in the vicinity of these

points. In the lowest order the value  $b_k(x_k)$  has to coincide with  $g_r(x_k)$ . However, in general  $g_r$  has some slope and could cut the boundary  $b_k$ . We consider the linear approximation  $g_r(x_k) + g'_r(x_k)(x - x_k) + \mathcal{O}((x - x_k)^2)$  and ask for  $\hat{x}$  such that

$$b_k(\hat{x}) = g_r(x_k) + g'_r(x_k)(\hat{x} - x_k) \quad (22)$$

is satisfied with exactly one solution. This corresponds to the case of smooth touching where both curves have the same tangent  $b'_k(\hat{x}) = g'_r(x_k)$ , which yields  $\hat{x}$  in (20). (19) follows from  $g_r(x_k) = b_k(\hat{x}) - g'_r(x_k)(\hat{x} - x_k)$ .

In addition to the error  $\mathcal{O}(f_s'''(x_k))$  the result  $\hat{x}$  comes with an error which can be estimated by  $\mathcal{O}((\hat{x} - x_k)^2) \leq \mathcal{O}(g'_r(x_k)^2)$ . This completes the assertion. ■

For  $\delta/r$  small enough and large  $s$  the derivatives of  $g_r$  and  $f_s$  will become small and the higher order correction  $\mathcal{O}(\varepsilon)$  will be negligible. The relations will be exploited in the calculation of essentially optimal  $f_s$ .

The relations (19) provide a complete characterization of the optimal stability polynomial only if the function  $g_r$  satisfy some additional conditions at the end points  $z = 0$  and  $z = -r$ . These conditions have to guarantee that the opening angle of the thin region is inside the stability domain at these end points. In principle these conditions can be checked after a possibly candidate for an optimal stability polynomial is calculated based on (19), see below.

The boundary of the second order stability domain generated by

$$f_s(z) = 1 + z + \frac{1}{2}z^2 + \sum_{k=3}^s \alpha_k z^k \quad (23)$$

is given implicitly by the relation  $|f_s(z)| = 1$ . For the behavior of the boundary at  $z = 0$  we consider  $z = -a + b\mathbf{i}$  for small  $a > 0$  and deduce

$$|b| = \sqrt[4]{\frac{8}{1 + 8(\alpha_4 - \alpha_3)}} a. \quad (24)$$

For the behavior at  $z = -r$  we consider

$$\tilde{f}_s(\tilde{z}) = f_s(\tilde{z} - r) = f_s(-r) + \sum_{k=1}^s \frac{f_s^{(k)}(-r)}{k!} \tilde{z}^k \quad (25)$$

at  $\tilde{z} = 0$ . The implicit relation  $|\tilde{f}_s(\tilde{z})| = 1$  gives for  $\tilde{z} = a + b\mathbf{i}$  in the case of small  $a > 0$

$$|b| = \sqrt{\frac{2|f_s'(-r)|}{f_s'(-r)^2 - |f_s''(-r)|}} a. \quad (26)$$

Hence, for the general case, we conclude that the function  $g_r$  should satisfy

$$|g_r(-a)| \leq \sqrt[4]{\frac{8}{1 + (f_s^{IV}(0) - 4f_s'''(0))/3}} a \quad \text{and} \quad |g_r(a - r)| < \sqrt{\frac{2f_s'(-r)}{f_s'(-r)^2 + f_s''(-r)}} a \quad (27)$$

for small  $a > 0$ .

### 3.4 Algorithm

We use the characterization given in Proposition 1 to formulate an algorithm which calculates the optimal second order stability polynomial  $f_s$  with  $s$  stages for a given thin region family.

The polynomial will be uniquely described by  $s - 2$  extrema at real positions labelled  $x_1 < x_2 < \dots < x_{s-2} < 0$ . The assumption of real extrema is inspired from the optimal real interval case, where also all extrema are along the real line. The following algorithm determines these initially unknown positions

$$X = \{x_k\}_{k=1}^{s-2}. \quad (28)$$

The derivative  $f'_s$  has the form

$$f'_s(z; X) = 1 + z + \sum_{k=2}^{s-1} \beta_k z^k \stackrel{!}{=} \left(1 - \frac{z}{x_{s-1}}\right) \prod_{k=1}^{s-2} \left(1 - \frac{z}{x_k}\right) \quad (29)$$

from which the remaining extremum

$$x_{s-1} = -\frac{1}{1 + \sum_{k=1}^{s-2} \frac{1}{x_k}} \quad (30)$$

follows as function of the given extrema  $X$ . The stability polynomial is now given by

$$f_s(z; X) = 1 + \int_0^z f'_s(\zeta; X) d\zeta \quad (31)$$

based on the  $s - 2$  extrema  $X$ .

For a given function  $g_r$  the stability polynomial  $f_s$  is characterized by the  $s - 2$  equations in (19). In the calculations it turned out that it suffices not only to neglect the second order error, but also the terms containing  $g'_r$  in (19).

It remains to formulate an expression for the value of  $r$  in dependance of  $X$ . We will assume that the boundary of the stability and the thin region coincide at  $z = -r$ , as in case i) with '=' in the working hypothesis. If  $f_s$  is constructed from  $X$  the boundary point on the real axis can easily be calculated by solving  $|f_s(r, X)| = 1$  which gives a function  $r = R(X)$ .

Altogether, we have to solve the following equations in order to obtain an optimal stability polynomial.

**Problem 2 (maximal thin region stability)** *Given  $g_r(z)$  and the unknowns  $X = \{x_k\}_{k=1}^{s-2}$ , solve the system of equations*

$$g_{R(X)}(x_k) = \sqrt{\frac{1 + f_s(x_k; X) \text{sign}(f''_s(x_k; X))}{|f''_s(x_k; X)|}}, \quad k = 1, 2, \dots, s - 2 \quad (32)$$

where  $R(X) < x_1$  such that

$$|f_s(R(X); X)| = 1, \quad (33)$$

for the unknown extrema positions  $X = \{x_k\}_{k=1}^{s-2} \subset \mathbb{R}$ .

Note, that the current formulation does not require any form of optimization since it is based on a direct characterization by a single system of equations. This system of non-linear equations was implemented in C and solved with the advanced quasi-Newton method provided by [15]. An appropriate initial guess is found by choosing  $g_r \equiv 0$  and the first order or second order maximal real interval result. For various shapes of thin regions a continuation method was employed.

To avoid round-off errors the derivative (29) was converted into a representation by Chebyshev-polynomials on a sufficiently large interval for each evaluation of the residual. The necessary differentiation, integration and evaluation was then performed on the Chebyshev coefficients. This method proved to be efficient and stable also for large values of  $s$ . However, for the applications in this paper only methods with  $s \leq 20$  were used.

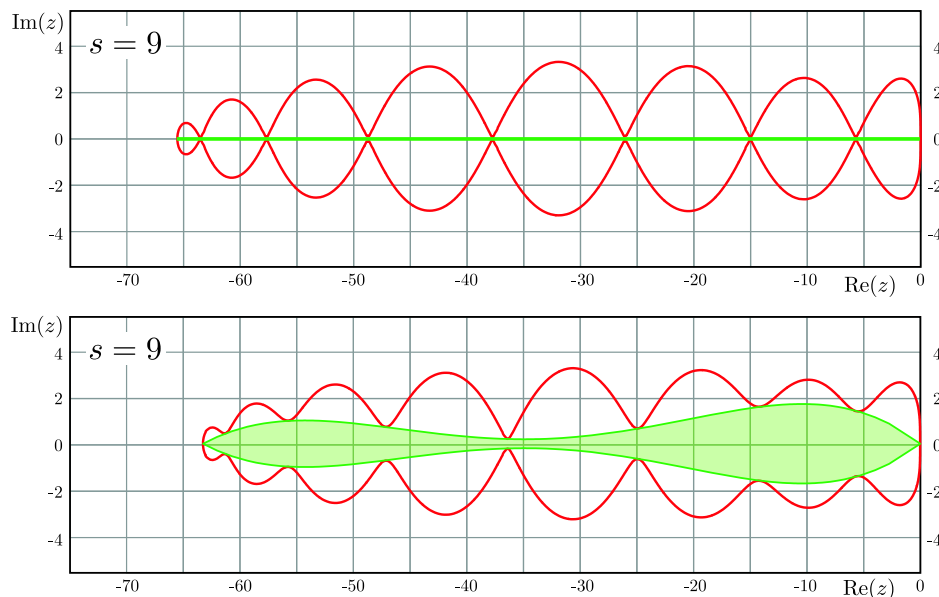


**Figure 4:** Two examples of thin regions, the real interval and a non-convex domain, together with their respective optimal stability region in the case  $s = 9$  and  $p = 2$ . The stability domains allow a maximal extension  $r$  along the real line for the particular shape. Note, that the second case requires a smaller value of  $r$ .

### 3.5 Examples

In this section we show several examples of optimal thin region stability polynomials in order to demonstrate the flexibility and usefulness of the proposed algorithm. We only present results for  $p = 2$ . Some of the examples must be considered as extreme cases of possible spectra.

Fig. 4 shows two optimal stability regions for  $s = 9$  for two different thin regions. The upper case is that of a real interval with no imaginary part. In both results the denting points reach down to the boundary of the thin region. The deeper they reach the longer the real extension. Hence, the lower example has a smaller value for  $r$ .

The thin region can be of almost arbitrary shape, even though the framework presented above is developed for well behaved regions. In Fig. 5 the thin region has been subdivided into relative regions of different thickness. In the upper plot the thin region is subdivided into parts with relations 1:2:1. In the lower plot the five parts have relations 1:3:2:3:1. The small parts have a thickness of 0.1, in contrast to 1.6 of the thick parts. The algorithm manages to find the optimal stability region in which the denting points touch the boundary of the thin region. Problems can occur when the side pieces of the rectangles cut the stability domain boundary. For that reason the first derivative of  $g_r$  should be sufficiently small in general.

In the last example we compare to the damping approach, see [1], [7], [20]. The thin region is given by a thin slot of thickness 0.1 but in the last 10% an ellipse of thickness 1.5 is installed. In the damping approach the optimal result for the real interval is modified by a constant factor  $< 1$  multiplied to the polynomial  $f_s$ . This leads to an ellipse-shape opening similar to that of example 2 above which is strongly reducing the real extension. The new approach controls every denting point individually and more flexible. In the current example it allows the denting points to be closer to the real line and, hence, produce a superior result with longer real size. The damping result is clearly not optimal and will require smaller time steps.

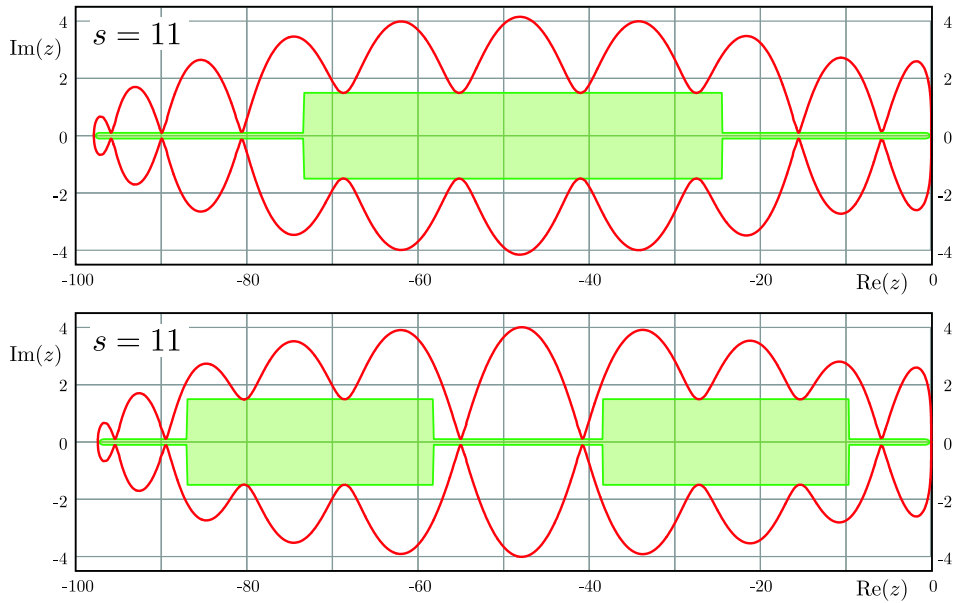


**Figure 5:** Two extreme examples to demonstrate the ability of the proposed algorithm to produce highly adapted essentially optimal stability regions. The rectangles occupy relative parts of the real extension and have a thickness of 1.6.

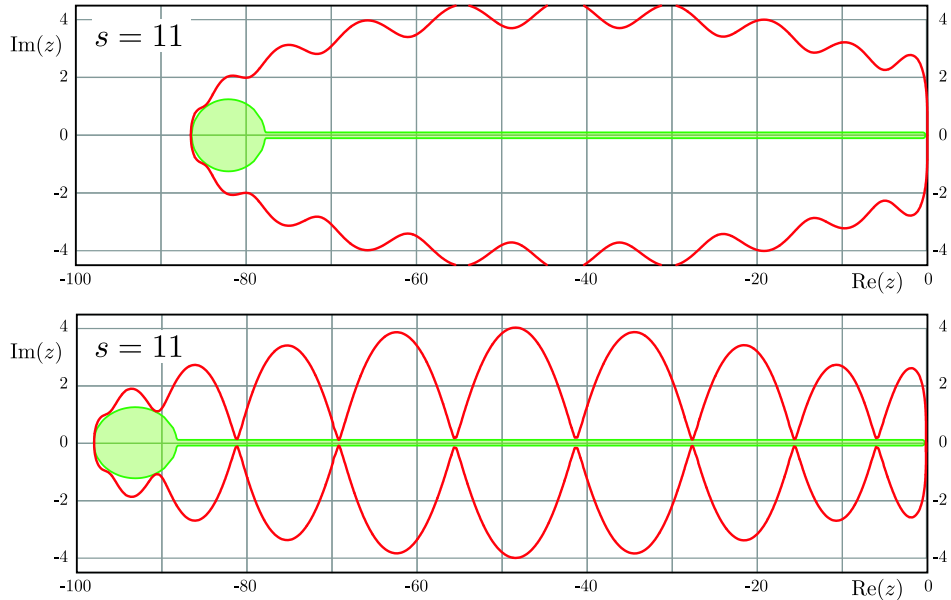


**Figure 6:** Comparison of damping strategies (top) to the new theory (bottom): The thin region is mostly very thin except for an ellipse at the left edge of the region. In the optimal stability domain produced by the new algorithm a clearly larger value of  $r$  is obtained. The damping result is much more open on the expense of a larger real extension.

## 4 Semi-discrete upwind finite volume methods

The theory given above shall be used to construct efficient explicit methods for the solution of hyperbolic-parabolic systems of balance laws. Such equations describe, for example, the flow of compressible, viscous fluids. We will focus on transport-dominated situations in which the use of upwind methods for the hyperbolic part is mandatory. The generic model will be the linear, scalar advection-diffusion equation. In the following we briefly describe the semi-discrete approach of upwind finite volume methods to fix notations. Both theoretical and numerical discussions of such systems can be found in the text books [3] by Godlewski and Raviart, [13] by LeVeque or [21] by Wesseling.

Here, we restrict ourselves to the one-dimensional case  $U : \mathbb{R} \times \mathbb{R}^+ \rightarrow \mathbb{R}^M$  with  $M$  the dimension of the state space. The generic hyperbolic-parabolic system is given by

$$\partial_t U + \partial_x F(U) = D(U) \partial_x U \quad (34)$$

with the hyperbolic flux function  $F(U) \in \mathbb{R}^M$ , and (semi-)definite diffusion matrix  $D(U) \in \mathbb{R}^{M \times M}$ . The basic discrete variable of finite volume methods is the cell average  $U_i^n$  of the unknown for a grid cell  $[x_{i-\frac{1}{2}}, x_{i+\frac{1}{2}}]$ ,  $i \in \mathbb{N}$  with length  $\Delta x$  at time level  $t^n$ . A semi-discrete formulation for (34) has the form

$$\partial_t U_i(t) = \frac{1}{\Delta x} \left( \tilde{F}_{i-\frac{1}{2}}^{(D)}(\hat{U}(t)) - \tilde{F}_{i+\frac{1}{2}}^{(D)}(\hat{U}(t)) \right). \quad (35)$$

with a numerical flux function  $\tilde{F}^{(D)}$  which approximates the diffusion and flux across the cell interface. Here,  $U_i(t)$  is the time-continuous cell average and the hat  $\hat{U} = \{U_i\}_{i \in \mathbb{N}}$  combines all averages. The resulting system forms a system of ordinary differential equations and can be solved with ODE methods.

In transport-dominated regimes the diffusive part is simply added as central difference to a hyperbolic upwind flux, viz.

$$\tilde{F}_{i+\frac{1}{2}}^{(D)}(\hat{U}) = \tilde{F}_{i+\frac{1}{2}}^{(hyp)} \left( U_{i+\frac{1}{2}}^{(-)}, U_{i+\frac{1}{2}}^{(+)} \right) - D_{i+\frac{1}{2}} \frac{U_{i+1} - U_i}{\Delta x} \quad (36)$$

where  $D_{i+\frac{1}{2}}$  is an approximation of the diffusion coefficient at the interface. This leads to a second order approximation of the diffusive part in the evolution equation. The hyperbolic upwind flux incorporates a Riemann solver for a left and right hand state at the interface, see [13]. Second order for the hyperbolic part is achieved using linearly reconstructed values for the left and right hand values  $U_{i+\frac{1}{2}}^{(\pm)}$  with gradient approximations  $\delta_i \hat{U} \approx (\partial_x U)_i$ . These will be zero for a first order scheme or given by central differences for a full second order scheme.

### 4.1 Advection-diffusion

By characteristic decomposition any hyperbolic system can be written locally as a set of decoupled advection equations. Many hyperbolic numerical methods are based on this fact. Hence, for the construction of the ODE method we will consider the scalar function  $u : \mathbb{R} \times \mathbb{R}^+ \rightarrow \mathbb{R}$  and the advection-diffusion equation

$$\partial_t u + a \partial_x u = D \partial_{xx} u \quad (37)$$

with a constant advection equation  $a \in \mathbb{R}$  and a positive diffusion constant  $D \in \mathbb{R}$ . In general the characteristic decomposition will not decouple the diffusive part of a system. In the model only the diagonal part is considered.

For advection with  $a > 0$  the standard upwind method gives  $\tilde{F}_{i+\frac{1}{2}}^{(hyp)} = a u_{i+\frac{1}{2}}^{(-)}$  for the hyperbolic flux. This expression is the basis for any highly developed numerical Riemann solver for hyperbolic systems. We obtain as diffusive flux

$$\text{1st order : } \quad \tilde{F}_{i+\frac{1}{2}}^{(D)}(\hat{u}) = a u_i - \frac{D}{\Delta x}(u_{i+1} - u_i), \quad (38)$$

$$\text{2nd order : } \quad \tilde{F}_{i+\frac{1}{2}}^{(D)}(\hat{u}) = a(u_i + \frac{1}{4}(u_{i+1} - u_{i-1})) - \frac{D}{\Delta x}(u_{i+1} - u_i). \quad (39)$$

In the case of first order we have  $\delta_i \hat{u} \equiv 0$ , while for second order,  $\delta_i \hat{u} = (u_{i+1} - u_{i-1})/(2\Delta x)$ .

## 4.2 Eigenvalue structure

The ODE system (35) with the flux function (38) or (39) shall be solved by an explicit Runge-Kutta method with an optimal stability domain. Therefore, the location of the eigenvalues in the complex plane needs to be investigated. The structure of the eigenvalue depends to some extent on the chosen boundary conditions, see e.g., the book by Kreiss and Ulmer [8]. Here, we only consider periodic boundary conditions as a first approach. The periodic case is widely used to obtain basic stability properties for numerical methods for hyperbolic problems. The investigation of different cases is left for future work.

The coupled system (35) with (38) or (39) is linear and has the form

$$\partial_t u_i(t) = \sum_j A_{ij} u_j(t) \quad (40)$$

with a constant matrix  $A$  containing the parameters  $a$ ,  $D$  and  $\Delta x$ . Standard Fourier analysis gives the linear equation

$$\partial_t v_k(t) = g(k \Delta x) v_k(t). \quad (41)$$

for the amplitude  $v_k(t)$  of the wave with wave number  $\xi = k \Delta x$  and the amplification factor  $g(\xi)$ . The function  $g$  depends on  $a$ ,  $D$  and  $\Delta x$  through  $A$  and is closely related to the amplification factor of the von-Neumann analysis of difference equations, see [3], [8], or [21]. For a time step size  $\Delta t$  we define the set of eigenvalues in the complex plane

$$G^{(1,2)} := \left\{ \Delta t g^{(1,2)}(\xi) \in \mathbb{C} \mid 0 \leq \xi \leq 2\pi \right\} \subset \mathbb{C} \quad (42)$$

where the superscript indicate the use of the first order (38) or second order flux (39). Since  $\Delta x > 0$  may vary arbitrarily we let  $\xi$  vary with real values in  $[0, 2\pi]$ . The shape of  $G$  is influenced by the two parameters

$$\lambda = \frac{a\Delta t}{\Delta x} \quad \text{and} \quad \kappa = \frac{2D}{a\Delta x} \quad (43)$$

based on the parameters of the method and the discretization. The parameter  $\lambda$  is the Courant number and  $\kappa$  describes an inverse grid-based Reynolds number. The main properties of  $G^{(1,2)}$  are summarized in the following lemma.

### Lemma 1 (Upwind eigenvalue structure)

(I) *First order case (35) with (38): The eigenvalues are given equivalently by*

$$\begin{aligned} G^{(1)} &= \{ \lambda((1 - \cos(\xi))(1 + \kappa) + \sin(\xi) \mathbf{i}) \in \mathbb{C} \mid 0 \leq \xi \leq 2\pi \} \\ &= \left\{ 2\lambda x \left( x(1 + \kappa) + \sqrt{1 - x^2} \mathbf{i} \right) \in \mathbb{C} \mid -1 \leq x \leq 1 \right\}. \end{aligned} \quad (44)$$

*The eigenvalues are placed symmetric to the real axis in the form of an ellipse touching  $z = 0$ . For  $z \in G^{(1)}$  the bounds of real and imaginary part are given by*

$$-2\lambda(1 + \kappa) \leq \text{Re}(z) \leq 0 \quad \text{and} \quad |\text{Im}(z)| \leq \lambda \quad (45)$$

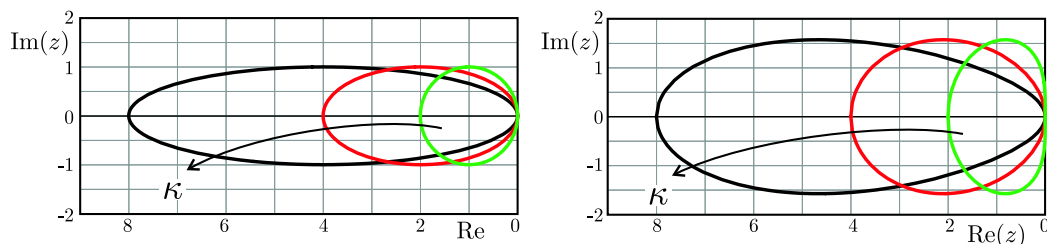


**Figure 7:** Positions of eigenvalues of first (left) and second (right) order diffusive upwind method for an advection-diffusion equation with varying value of  $\kappa = \frac{2D}{a\Delta x}$  and  $\lambda = 1$ . For large values of  $\kappa$  the eigenvalues define a thin region along the real axis.

and the maximal imaginary part is uniquely reached when  $\text{Re}(z) = -\lambda(1 + \kappa)$ .

(II) Second order case (35) with (39): The eigenvalues are given equivalently by

$$\begin{aligned} G^{(2)} &= \left\{ \lambda \left( (1 + 2\kappa - \cos(\xi)) \sin\left(\frac{\xi}{2}\right)^2 + \frac{1}{4}(6 \sin(\xi) - \sin(2\xi)) \mathbf{i} \right) \in \mathbb{C} \mid 0 \leq \xi \leq 2\pi \right\} \\ &= \left\{ 2\lambda x \left( x(x^2 + \kappa) + (1 + x^2)\sqrt{1 - x^2} \mathbf{i} \right) \in \mathbb{C} \mid -1 \leq x \leq 1 \right\}. \end{aligned} \quad (46)$$

The eigenvalues are placed symmetric to the real axis in the form of a distorted ellipse touching  $z = 0$ . For  $z \in G^{(2)}$  the bounds of real and imaginary part are given by

$$-2\lambda(1 + \kappa) \leq \text{Re}(z) \leq 0 \quad \text{and} \quad |\text{Im}(z)| \leq \lambda \frac{9 + \sqrt{17}}{16} \sqrt{\frac{3}{2}\sqrt{17} - \frac{5}{2}} \approx 1.574\lambda \quad (47)$$

and the maximal imaginary part is uniquely reached when  $\text{Re}(z) = -\lambda(9 + 4\kappa + (1 + \kappa)\sqrt{17})/16$ .

These properties can be verified by a thorough calculation. The equivalence of the representations through  $\xi$  or  $x$  is seen by substituting  $x = \sin \frac{\xi}{2}$ . We note, that the imaginary part is not affected by the parameter  $\kappa$ , i.e., by the diffusive part. However, the imaginary part is larger for the second order case. The coverage of the real axis is mainly controlled by the diffusion parameter  $\kappa$ . This is in accordance to the fact that diffusion introduces increasing real eigenvalues to a system. However, the presence of advection leads to an ellipsoidal arrangement of the eigenvalues away from the real axis. Furthermore, even if no diffusion is considered,  $\kappa = 0$ , the eigenvalues have non-vanishing real parts and no purely imaginary values occur. This is due to upwinding which introduces diffusion into the numerical method.

The locations of the eigenvalues for  $\lambda = 1$  and increasing values of  $\kappa = 0, 1, 3$  are depicted in Fig. 7 for both the first and second order case. For increasing values of  $\kappa$  the region is stretched along the real axis but keeps its maximal imaginary value. The thicker extension of the second order case (right hand plot) is clearly visible.

## 5 Stabilized advection-diffusion

For large  $\kappa$  the eigenvalues of the semi-discrete upwind method for advection-diffusion define a narrow region around a large interval of the real axis. This makes the former results of thin region stability domains applicable.

### 5.1 Identifying thin regions

We are looking for the defining function  $g_r$  of a thin region in the form

$$G_r = \{z = a + b\mathbf{i} \in \mathbb{C} \mid |b| \leq g_r(a)\} \quad (48)$$

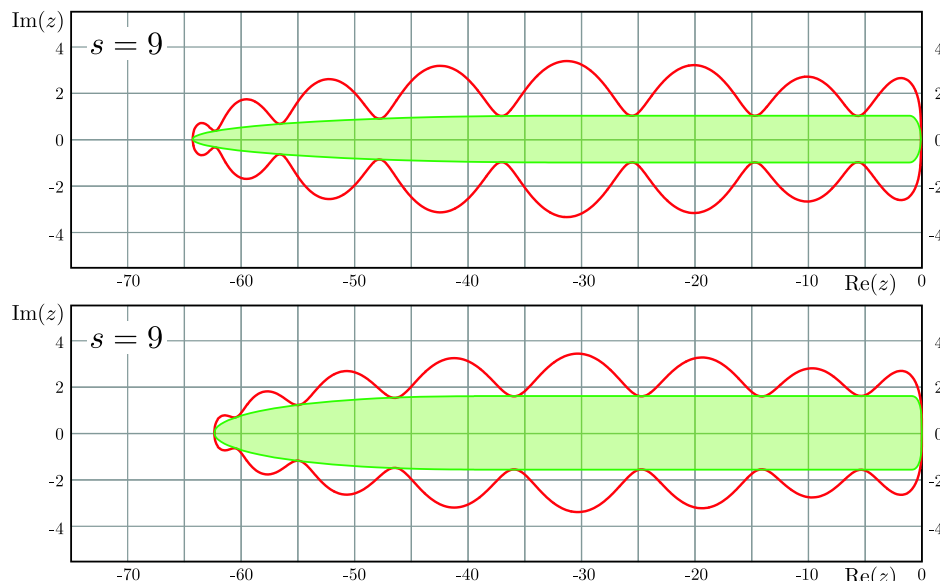


**Figure 8:** The optimal second order stability domains for semi-discretized advection-diffusion for  $s = 9$  in the case of spatially first order (top) and spatially second order (bottom). Note, that the second case requires a smaller value of  $r$  since the thin region extends further into the imaginary plane.

as in Definition 1 which includes the eigenvalues  $G^{(1,2)}$ . The eigenvalues (46) of the second order case are spanned by the positive and negative values of the function

$$\bar{g}^{(2)}(a, \lambda, \kappa) = \lambda \left( 2 + \sqrt{2 \frac{|a|}{\lambda} + \kappa^2} - \kappa \right) \sqrt{\frac{1 + \kappa}{2} \left( \sqrt{2 \frac{|a|}{\lambda} + \kappa^2} - \kappa \right) - \frac{|a|}{2\lambda}} \quad (49)$$

which depends on the parameters  $\kappa$  and  $\lambda$ . In principle, for a fixed choice of  $\kappa$  and  $\lambda$  no points of the interior of the shape is an eigenvalue. However, in the computation of a general non-linear system various advection velocities and diffusion coefficients are present in a single time step. Hence, in general we consider  $0 < \lambda < \lambda_{\max}$ ,  $0 < \kappa < \kappa_{\max}$  and take the hull of all shapes generated by  $\bar{g}^{(2)}(a, \lambda, \kappa)$  for the various values of  $\kappa$  and  $\lambda$ . In the following we will assume  $\lambda_{\max} = 1$  which means that the time step shall resolve the advection scale on the current grid, i.e.,  $\Delta t \approx a \Delta x$ . In principle,  $\lambda_{\max} > 1$  is possible allowing time steps larger than those of the traditional CFL condition.

For the second order case we obtain the generating function

$$g_{r(\kappa)}^{(2)}(a) = \begin{cases} (2 + \sqrt{2|a| + \kappa^2} - \kappa) \sqrt{\frac{1+\kappa}{2} (\sqrt{2|a| + \kappa^2} - \kappa) - \frac{1}{2}|a|}, & -r(\kappa) \leq a < -r_0(\kappa) \\ \frac{9 + \sqrt{17}}{16} \sqrt{\frac{3\sqrt{17}-5}{2}}, & -r_0(\kappa) \leq a < -r_0(0) \\ (2 + \sqrt{2|a|}) \sqrt{\frac{1}{2}(\sqrt{2|a|} - |a|)}, & -r_0(0) \leq a \leq 0 \end{cases} \quad (50)$$

where we dropped the index max from the parameter  $\kappa$  and write

$$r(\kappa) = 2(1 + \kappa) \quad \text{and} \quad r_0(\kappa) = \frac{9 + 4\kappa + (1 + \kappa)\sqrt{17}}{16} \quad (51)$$

For reference we state the behavior of  $g_{r(\kappa)}^{(2)}$  at the end points  $a = 0$  and  $a = -r$ . Asymptotic analysis yields

$$g_{r(\kappa)}^{(2)}(-a) = \sqrt[4]{8a} \quad \text{and} \quad g_{r(\kappa)}^{(2)}(-r(\kappa) + a) = \sqrt{\frac{8}{2 + \kappa} a} \quad (52)$$

$s$	$r_{\max}$	$r_{\max}/s^2$	$s$	$r_{\max}$	$r_{\max}/s^2$
2	2.0	0.5	10	79.686	0.7968
3	5.806	0.6451	20	322.997	0.8074
4	11.477	0.7173	30	728.505	0.8094
5	18.812	0.7524	40	1296.212	0.8101
6	27.743	0.7706	50	2026.142	0.8104
7	38.296	0.7815	70	3972.470	0.8107
8	50.471	0.7886	90	6567.642	0.8108
9	64.268	0.7934	100	8108.547	0.8108

**Table 1:** Maximal real interval  $[-r_{\max}, 0]$  included in the stability regions of  $f_s$  for the thin region of the spatially first order case  $g^{(1)}$ .

for small  $a$ . For the first order eigenvalues  $G^{(1)}$  the generating function of the hull is given by

$$g_{r(\kappa)}^{(1)}(a) = \begin{cases} \sqrt{\frac{|a|}{1+\kappa} \left(2 - \frac{|a|}{1+\kappa}\right)}, & -r(\kappa) < a < -(1+\kappa) \\ 1, & -(1+\kappa) < a < -1 \\ \sqrt{|a|(2-|a|)}, & -1 < a < 0 \end{cases} \quad (53)$$

with  $r(\kappa)$  as above. The asymptotic behavior at the end points is given by

$$g_{r(\kappa)}^{(1)}(-a) = \sqrt{2a} \quad \text{and} \quad g_{r(\kappa)}^{(1)}(-r(\kappa) + a) = \sqrt{\frac{2}{1+\kappa}a} \quad (54)$$

for small  $a$ .

## 5.2 Optimal stability polynomials

The optimal stability polynomials  $f_s$  for fixed  $s$  for (50)/(53) are calculated by the algorithm described in Sec. 3.4. As example the results for  $s = 9$  for both the first and second order case are displayed in Fig. 8. As expected a thicker region requires a shorter real interval. The maximal real interval is only possible when no extension into the imaginary part of the complex plane is present. For  $s = 9$  the maximal real interval  $[-r_{\max}, 0]$  included for the second order case is  $r_{\max} \approx 62.2$  which allows  $\kappa \approx 30.1$ . For the first order case the values  $r_{\max} \approx 64.3$  and  $\kappa \approx 31.15$  are somewhat higher.

We may check the asymptotics of the end points of the stability domains using the results of the end of Sec. 3.3. By inspection of the second order results we find  $\alpha_k > 0$  and  $\alpha_4 < \alpha_3$  for all computed  $s$ , hence, we have  $|b| \geq \sqrt[4]{8a}$  for the domain boundary at the origin. At the tip of the domain we have  $|f'_s(-r)| \leq \frac{5}{2}$  and  $|f''_s(-r)| \geq \frac{5}{4}$  for  $s > 4$ . Hence, it follows  $|b| \geq \sqrt{a}$  which is enough for  $\kappa > 6$ , according to the asymptotic behavior given above. For  $s = 2, 3, 4$  the correct behavior at  $z = -r$  can be checked case by case.

For the current paper the optimal stability polynomial for the first and second order diffusive upwind has been calculated for  $s = 3, \dots, 101$ . Except for the lower cases  $s = 3, 4$  all polynomials were obtained from solving the equations in Problem 1. The low cases do not exhibit a thin region due to small values of  $\kappa$  and the optimal polynomials have been found by a separate optimization. In principle stability polynomials for higher values of  $s$  could also be obtained.

For the case of a pure real interval the relation  $r_{\max} \approx s^2$  has been reported, e.g., in the work of [1]. For the present results the maximal value  $r_{\max}$  and the quotient  $r_{\max}/s^2$  are displayed in Table 1 for the spatially first order and in Table 2 for the spatially second order case. The numbers suggest the relations  $r_{\max} \approx 0.81 s^2$  and  $r_{\max} \approx 0.79 s^2$ , respectively.

$s$	$r_{\max}$	$r_{\max}/s^2$	$s$	$r_{\max}$	$r_{\max}/s^2$
2	2.0	0.5	10	77.321	0.7732
3	4.520	0.5022	20	315.949	0.7898
4	10.552	0.6595	30	713.359	0.7926
5	17.690	0.7076	40	1269.691	0.7935
6	26.447	0.7346	50	1984.962	0.7939
7	36.782	0.7507	70	3892.310	0.7943
8	48.707	0.7610	90	6435.433	0.7944
9	62.220	0.7682	100	7945.410	0.7945

**Table 2:** Maximal real interval  $[-r_{\max}, 0]$  included in the stability regions of  $f_s$  of the thin region for the spatially second order case  $g^{(2)}$ .

### 5.3 Method construction

Once the stability polynomials are known it remains to construct a practical Runge-Kutta method for the ODE

$$y'(t) = F(y(t)) \quad (55)$$

from the polynomial coefficients.

We will use a variant of the algorithm given in [1], where the recursive formula for an orthogonal representation of the stability polynomial was used supplemented by a second order finishing procedure. For our application it turned out to be sufficient to replace the orthogonal recursion steps by a combination of Euler steps of increasing step sizes. The second order finishing procedure remains the same. The final algorithm is given by

**Algorithm 1 (increasing Euler steps)** *Given initial data  $y_n$  at time level  $n$ . Let  $y^{(0)} = y_n$ .*

$$\begin{aligned} y^{(j+1)} &= y^{(j)} + \alpha_{j+1} \Delta t F(y^{(j)}), \quad j = 0, 1, 2, \dots, s-2 \\ y_{n+1} &= y^{(s-1)} + \alpha_{s-1} \Delta t F(y^{(s-1)}) + \sigma \left( F(y^{(s-1)}) - F(y^{(s-2)}) \right) \end{aligned} \quad (56)$$

The parameters become obvious when the form

$$f_s(z) = (1 + \beta_1 z + \beta_2 z^2) \prod_{k=1}^{s-2} \left( 1 - \frac{z}{z_k} \right) \quad (57)$$

of the stability polynomial is used. The Euler steps are obtained from the real zeros  $\alpha_j = -\frac{1}{z_j}$ ,  $j = 1, 2, \dots, s-2$  while the second order procedure represents the part containing the complex zeros and we find  $\alpha_{s-1} = \beta_1/2$  and  $\sigma = 2\beta_2/\beta_1 - \beta_1/2$ . Note that an implementation with only one temporary storage variable is possible.

The finishing procedure allows to incorporate an error estimation. However, in time-explicit fluid simulations the time step is usually chosen such that wave phenomena are resolved during the time step. This is an accuracy condition and implies the CFL condition  $\Delta t \approx c^{(\max)} \Delta x$ , so that any wave propagates only one cell. An error estimation is most commonly based on the spatial error and spatial refinement and the time step is chosen according to the transport resolving CFL condition. Hence, we do not consider temporal error estimation in the current paper.

#### 5.3.1 Internal stability

A problem to address while constructing the Runge-Kutta method is the question of stability of the internal stages. Any Runge-Kutta method is built on internal stages which are more or less

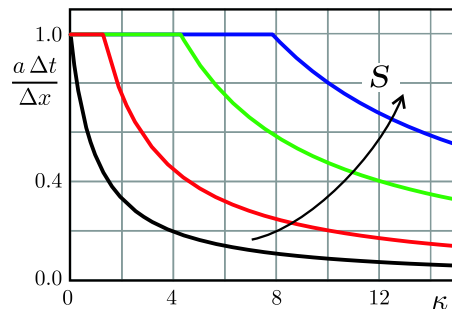


**Figure 9:** Time step constraints for advection-diffusion for stabilized explicit Runge-Kutta methods with stages  $s = 2, 3, 4, 5$  drawn over the diffusion parameter  $\kappa = 2D/(a\Delta x)$ .

made up out of single update steps. For problems with thin region spectra successive iteration of a single explicit Euler update of the form  $y + \tau F(y)$  is stable only for a very small time step  $\tau$ . Within the stages of a method with optimized stability polynomials single update steps with time steps  $\tilde{\tau} > \tau$  may accumulate and lead to internal instabilities. Only the proper over-all update is proven to be stable.

In order to relax the problem of internal instabilities, a special ordering of the internal steps during one full time step is preferable. This is investigated in the work [11] from Lebedev, see also the discussion in [5]. Here we interchange steps with large and small step sizes and start with the largest one. The result yields a practical and efficient method as shown in the numerical examples in the next section for advection-diffusion and viscous, compressible flow.

## 6 Numerical experiments

In the following we investigate the numerical performance of the derived scheme for advection-diffusion equations. The implementation considers only the spatially second order case (35) with (39) and the stabilized Runge-Kutta method uses increasing Euler steps as in Algorithm 1. After the results for the linear case we also present some results for the application of the stabilized methods to the non-linear system of compressible fluid dynamics.

### 6.1 Linear equation

The parameters of the explicit Runge-Kutta methods derived above have been calculated with high precision and implemented in order to solve an instationary problem of advection-diffusion. Due to the special design of the method and the possibility of choosing the optimal number of stages according to the strength of the diffusion, i.e., the value of  $\kappa$ , the time step during the simulation is fully advection-controlled.

For fixed  $s$  the time step of the method has to satisfy

$$\frac{a \Delta t}{\Delta x} \leq CFL \cdot \lambda_{\max}^{(s)}(\kappa) \quad (58)$$

with

$$\lambda_{\max}^{(s)}(\kappa) = \min \left( 1, \frac{r_{\max}^{(s)}}{2(\kappa + 1)} \right) \quad (59)$$

where  $\kappa = 2D/(a\Delta x)$  as above. For time and space depended values of  $a$  and  $\kappa$ , this procedure provides an adaptive time step control as proposed, e.g., in [13] for hyperbolic problems. The value of  $r_{\max}^{(s)}$  is given for each method. The number  $CFL \leq 1$  allows to increase the robustness

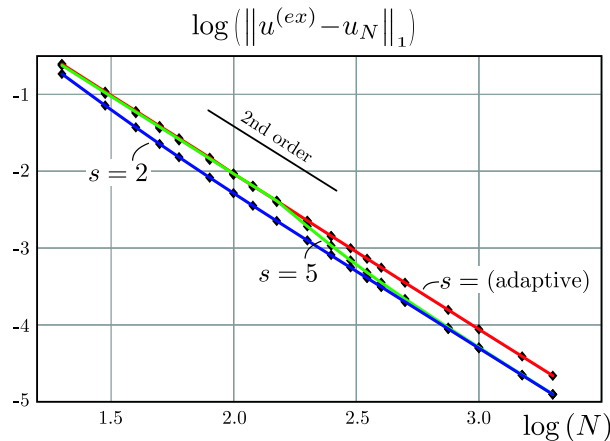


**Figure 10:** Error curves of second order upwind/central-difference finite volume method for advection-diffusion with stabilized explicit Runge-Kutta time integration. The initial condition is (61) and the diffusion coefficient  $D = 0.1$ .

of the method by reducing the time step below the marginally stable value. We suggest the usage of  $CFL \approx 0.9$ , which is common when calculating hyperbolic problems. In Fig.9 the graphs of  $\lambda_{\max}^{(s)}$  for  $s = 2, 3, 4, 5$  are drawn. We can see that the range of the diffusion parameter  $\kappa$  in which a pure advection time step  $a\Delta t/\Delta x = 1$  is allowed grows with  $s$ . However, for larger  $s$  also more internal grid updates are needed. Hence, in a *stage-adaptive calculation* the number of stages  $s$  is chosen such that the method just reaches the kink in Fig.9 for the current value for  $\kappa$ . The optimal  $s$  is given by

$$s^{(\text{opt})} = \min \left\{ s \mid \lambda_{\max}^{(s)}(\kappa) = 1 \right\}. \quad (60)$$

This assures maximal efficiency. The source code is available online, see [18].

We solve the time evolution for the initial conditions

$$u_0(x) = 4 + \frac{8}{\pi} \left( \sin\left(\frac{\pi}{2}x\right) + \frac{2}{3} \sin\left(\frac{3\pi}{2}x\right) \right) \quad (61)$$

on the interval  $x \in [-2, 2]$  with periodic boundary conditions up to time  $t = 0.8$ . Advection velocity is  $a = 1$  and various diffusion coefficients in the advection dominated regime between  $D = 0.001$  and  $D = 1.0$  have been considered. The exact solution for these cases are easily found by analytic methods.

For values of  $CFL = 0.95$  or  $CFL = 0.99$  all methods for various  $s$  were second order convergent and stable. Here, we show detailed graphs of the case  $D = 0.1$ . Fig. 10 shows the error curves over spatial resolution in the cases  $s = 2$ ,  $s = 5$  and the stage-adaptive method. The stage adaptive method uses the optimal number of stages and  $s = 17$  is reached for the finest grid. A general second order empirical convergence is observable. Note, that increasing the spatial resolution also increases the value of  $\kappa$ . There is a slight change of error behavior of a method with fixed stages when it enters the "diffusion regime", i.e., the second term  $\sim (1 + \kappa)^{-1}$  in (59) becomes dominant. For  $s = 2$  in the present example this is the case already for coarse grids, while the stage-adaptive method stays in the "advection-regime". For  $s = 5$ , however, the transition happens at  $\log(N) \approx 2.3$  and from Fig. 10 we can see the error curve moving to the  $s = 2$  curve exhibiting a slightly smaller error constant.

The method in which the number of stages is chosen adoptively according to the value of  $\kappa$  integrates the equation with a time step which is purely derived from the advection. This time step is much larger than that required from a non-stabilized classical method as the method with

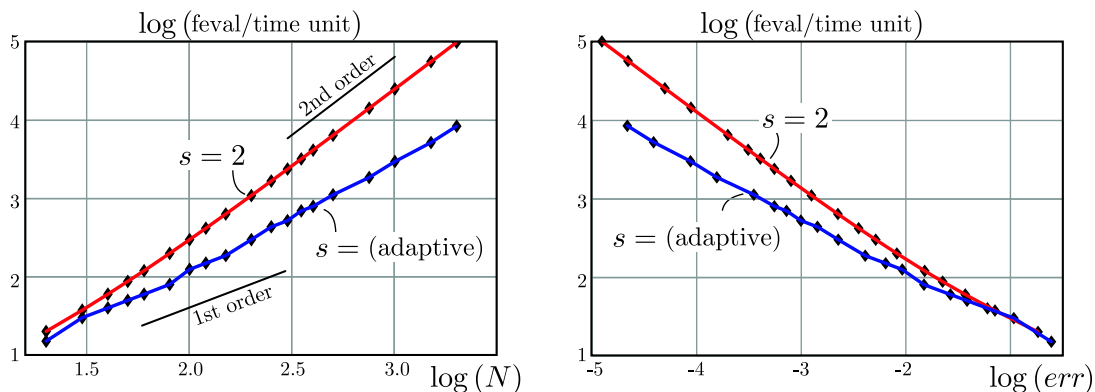


**Figure 11:** Comparison of necessary work for a specific resolution (left) or a specific error (right) in the case of a classical method  $s = 2$  and the new stabilized adaptive time stepping.

$s = 2$ , especially when  $D$  and/or the grid resolution is large. Also the efficiency increases since fewer function evaluations are needed as shown above. For the present case with  $D = 0.1$  the two plots in Fig. 11 compare the stage-adaptive stabilized method with the classical method  $s = 2$  in terms of efficiency. Both plots show the number of grid update evaluations for a calculation up to  $t = 1$  on the ordinate. The first plot relates the number of evaluations to the grid resolution and the second to the achieved error. For high resolution or small errors the adaptive method requires an order of magnitude less work. For the adaptive method the work is approximately  $\approx \mathcal{O}(N)$  which shows the linear scaling of an advection time step. The speed-up against the classical scheme is even increased for higher values of the diffusion coefficient or finer grids.

## 6.2 Compressible, viscous gas dynamics

Compressible, viscous gas dynamics in one space dimension considers the variable set  $U = \{\rho, v, T\}$ , that is, the density, velocity and temperature of the gas. The non-linear system describing its flow contains the conservation laws of mass, momentum and energy, viz.

$$\begin{aligned} \partial_t \rho + \partial_x \rho v &= 0 \\ \partial_t \rho v + \partial_x (\rho v^2 + p) &= \partial_x \left( \frac{4}{3} \mu \partial_x v \right) \\ \partial_t E + \partial_x (v(E + p)) &= \partial_x \left( \lambda \partial_x T + v \frac{4}{3} \mu \partial_x v \right) \end{aligned} \quad (62)$$

with ideal constitutive relations

$$E = \frac{1}{\gamma - 1} p + \frac{1}{2} \rho v^2, \quad p = \rho T. \quad (63)$$

The temperature is considered in energy units, i.e., the specific gas constant in the pressure law is unity. The adiabatic coefficient is set  $\gamma = \frac{5}{3}$  in the following calculations. On the right hand side of (62) the relations of Navier-Stokes and Fourier for the stress and heat flux have been included. They represent the diffusive or dissipative extension of the ideal Euler system of the left hand side. See the text books [3], [13], and [21] for a description of compressible fluid dynamics. The viscosity coefficient  $\mu$  and the heat conductivity  $\lambda$  ( $\lambda$  is also in energy units) shall be related by  $\lambda/\mu = \frac{15}{4}$  which is in accordance to a Prandtl number of  $\text{Pr} = \frac{2}{3}$ . The viscosity coefficient and heat conductivity are complicated functions of temperature in general. Here, we take

$$\mu(T) = \mu_0 T / T_0 \quad (64)$$

with a reference value  $\mu_0$  at  $T_0$ .

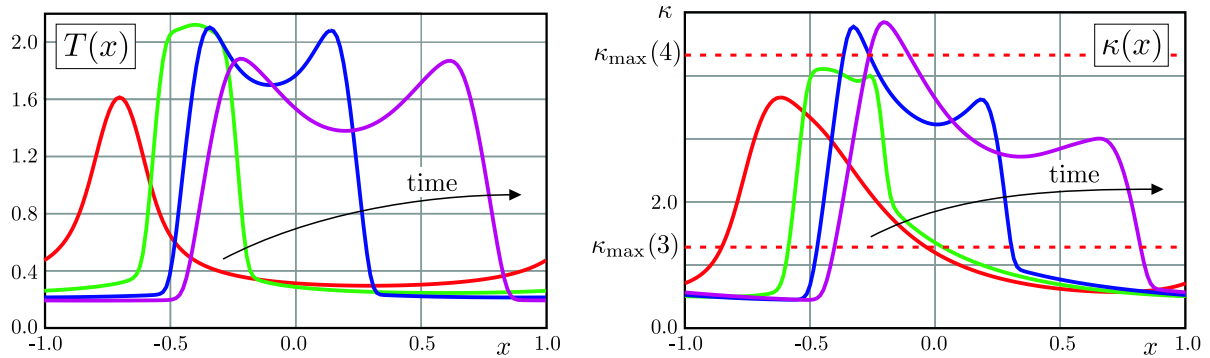


**Figure 12:** Evolution of an initially smooth temperature profile in compressible, viscous fluid dynamics with  $M_0 = 1/\sqrt{\gamma}$  and  $\text{Re} = 20$ . Initially the time integration uses 4 stages but increases to 5 stages once the  $\kappa$  reaches a maximal value.

If the space and velocity variable are scaled with a certain observation length and velocity scales  $\hat{x} = x/x_0, \hat{v} = v/v_0$  we assume the time scaling to be correspondingly  $\hat{t} = t/t_0$  with  $x_0/t_0 = v_0$  and  $v_0 = \sqrt{T_0}$ . With reference values we define  $\hat{\rho} = \rho/\rho_0$  and  $\hat{T} = T/T_0$  and derive the scaled momentum equation

$$\partial_{\hat{t}} \hat{\rho} \hat{v} + \partial_{\hat{x}} (\hat{\rho} \hat{v}^2 + \hat{p}) = \partial_{\hat{x}} \left( \frac{4}{3} \frac{\hat{T}}{\text{Re}} \frac{1}{\text{Re}} \partial_{\hat{x}} \hat{v} \right). \quad (65)$$

Mass and energy balance can be found analogously. The momentum equation is shown in order to introduce Reynolds number, which is defined by

$$\text{Re} = \frac{v_0 x_0}{\mu_0 / \rho_0} \quad (66)$$

based on reference values. In convection-dominated flow problems the Reynolds number is in the range  $\text{Re} > 1$  and may easily go up to  $10^5$ - $10^8$ .

An instationary process of the system (62) is solved by a finite volume method with upwinding and explicit time stepping, see [13]. The role of the advection velocity is taken by the highest characteristic velocity  $c_j = |\hat{v}_j| + \sqrt{\gamma \hat{T}_j}$  in a grid cell  $j$  and the respective maximum  $c = \max_{j \in \text{grid}} (c_j)$ . For the results in the following a standard Riemann solver for the inviscid equations has been implemented.

The viscous terms are added by central differences to the flux as in (36). In order to apply and control the newly derived stabilized Runge-Kutta method an expression for the diffusion scale  $\kappa$  must be found for the system (62). As first try, we propose an ad hoc expression which results from basic comparison of the heat conduction term in the scaled energy balance with the advection-diffusion equation. Since  $\lambda = \frac{16}{4} \mu$  we assume that the heat conduction is dominant in the dissipative terms. We suggest to use

$$\kappa_j = C \frac{5}{2} \hat{T}_j \frac{1}{\text{Re}} \frac{1}{c_j \Delta x} \quad (67)$$

with  $C = \mathcal{O}(1)$  and its global maximum  $\kappa = \max_{j \in \text{grid}} (\kappa_j)$  to control the stages of the stabilized method. As direct extrapolation of the above results we use

$$\frac{c \Delta t}{\Delta x} \leq CFL \cdot \lambda_{\max}^{(s)}(\kappa) \quad (68)$$

with (59) to control the time step in the calculations. Note, that  $c$  and  $\kappa$  are time depended and the time step may vary adaptively during a simulation.

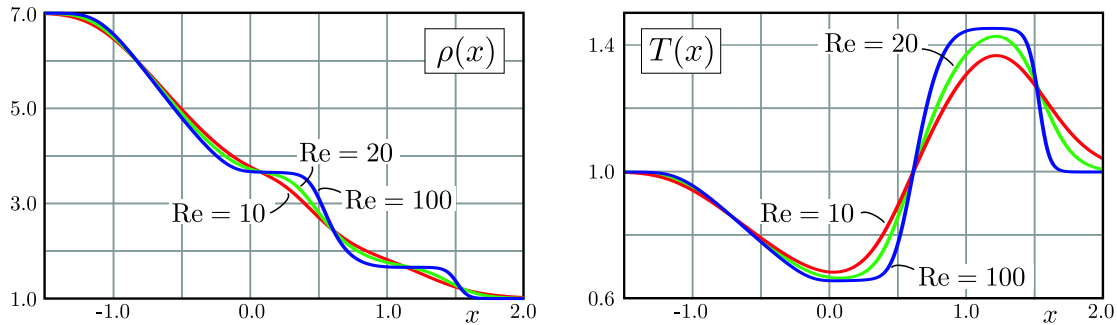


**Figure 13:** Solution of a Riemann problem in gas dynamics at time  $t = 0.8$  with different values for the Reynolds number,  $\text{Re} = 10, 20, 100$ . The plots show density (left) and temperature (right).

This strategy proved to be useful in the following examples and shows the applicability of the stabilized methods to the system (62). However, a detailed investigation and thorough derivation of the control parameters for linear and non-linear hyperbolic-parabolic systems remain for future work.

**Smooth numerical example:** As a first example we consider the smooth initial conditions

$$\rho(x, 0) = 2 + \frac{1}{2} \cos(\pi x), \quad v(x, 0) = 3 + \frac{5}{2} \sin(\pi x) \quad (69)$$

with  $p(x, 0) = 1$  on a periodic domain  $x \in [-2, 2]$  and calculate the time evolution up to  $t = 0.4$  with  $\text{Re} = 20$ . In this example we could take  $CFL = 0.95$  and  $C = 1$  in (67) over a wide range of grids and also different values of  $\text{Re}$  without observing stability problems of the stabilized Runge-Kutta method.

During the calculation the initial sin-function steepens to form two shock waves. It is interesting that during the evolution the value of  $\kappa$  increases and the time integration has to increase the number of stages in order to provide an advection time step. The curves for temperature and  $\kappa$  for different times  $t = 0.1, 0.2, 0.3, 0.4$  and  $x \in [-1, 1]$  are shown in Fig. 12. The grid resolution is  $\Delta x = 1.33 \times 10^{-2}$  and in the beginning we have  $\kappa \approx 3.5$ . The time integration uses  $s = 4$  initially, since  $\kappa_{\max}(s = 3) \leq \kappa \leq \kappa_{\max}(s = 4)$ . Between  $t = 0.2$  and  $t = 0.3$  the value of  $\kappa$  reaches the maximal value  $\kappa_{\max}(s = 4)$  related to  $r_{\max}$  by  $\kappa_{\max} = r_{\max}/2 - 1$  and has to switch to  $s = 5$ .

In this smooth example with 300 cells and  $\Delta x = 1.33 \times 10^{-2}$  the adaptive stabilized Runge-Kutta method used 189 time steps with 4 and later 5 stages. This results in  $\approx 860$  grid evaluations. The classical method with  $s = 2$  needs 974 time steps and 1988 grid evaluations which shows a speed-up of factor 2. If the grid is doubled the number of time steps are doubled to 378 for the adaptive method, but the stages are now between 5 and 6. This gives  $\approx 2080$  evaluations in contrast to 7050 for the  $s = 2$  method and the speed-up factor is 3.5.

**Discontinuous numerical example:** The Riemann problem with discontinuous initial data like

$$\rho(x, 0) = \begin{cases} 1 & x > 0 \\ 7 & x < 0 \end{cases}, \quad p(x, 0) = \begin{cases} 1 & x > 0 \\ 7 & x < 0 \end{cases} \quad (70)$$

with  $T(x, 0) = 1$  is a popular process in gas dynamics. It represents a shock tube experiment and in its evolution characteristic wave configurations occur. We use a grid  $x \in [-2.0, 3.0]$  with 500 points and open boundary with the end time  $t = 0.8$ . Fig. 13 shows the result of density and temperature for Reynolds numbers  $\text{Re} = 10, 20, 100$ . The results are obtained with the stabilized Runge-Kutta scheme with 360 time steps for all Reynolds numbers. The number of stages used decreased for increasing Re-number and in this case  $s = 8, 6, 4$  were necessary. However, due to

stability problems the CFL number had to be reduced to  $CFL = 0.5$  in these calculations. This could be a requirement due to the use of non-linear limiters which was necessary to handle the discontinuous initial conditions and to prevent spurious oscillations. It might also indicate that the use of the relation (67) is not yet optimal to control the stabilized method in the full non-linear systems case. Nevertheless, the current extension already provide a considerable speed-up over classical explicit methods.

## 7 Conclusion

The idea of optimized explicit Runge-Kutta methods in which additional stages stabilize the method has been extended to more general-shaped maximal stability domains. Guided by the classical results of a maximal disk and maximal real interval we introduced the concept of a *thin region* which is a symmetric domain around the real line with high aspect ratio. A general characterization of the optimal stability polynomial for thin regions is given. Specific cases could be investigated analytically, however, the general statement for the characterization of those optimal methods is not proven rigorously yet. Nevertheless, it could be used to derive a straight-forward algorithm to calculate a stability polynomial which is expected to be essentially optimal. Due to the direct characterization the optimal polynomial is described by a system of non-linear equations not involving any optimization. Several examples of optimized thin regions demonstrated the capabilities of the approach.

As interesting application of the new methods we presented semi-discrete finite volume upwind discretizations of advection-diffusion and studied their eigenvalue structure. After identifying the thin region character of these ODE systems, optimized Runge-Kutta stability polynomials for advection-diffusion could be calculated based on the direct characterization.

Equipped with the detailed knowledge about stability control and optimized time integration methods we presented numerical experiments for the advection-diffusion equation and non-linear viscous gas flows in one space dimension. Clear reduction of computational work in comparison to classical explicit methods could be observed. The time step remains advection-controlled also in the presence of diffusive gradients.

Future studies will include the application to multi-dimensional cases and the detailed investigation of stability properties of general hyperbolic-parabolic systems as well as the proof of the general characterization conjecture for thin regions. It will also be interesting to find applications with different and more involved thin region behavior.

**Acknowledgement:** The authors thank Ernst Hairer (University of Geneva) for pointing out reference [16] to us. The first author was supported by the German National Science Foundation (Deutsche Forschungsgesellschaft, DFG).

## References

- [1] A. Abdulle and A. A. Medovikov, *Second Order Chebyshev Methods Based on Orthogonal Polynomials*, Numer. Math. **90**, (2001), p.1-18
- [2] A. Abdulle, *Fourth order Chebyshev methods with recurrence relation*, SIAM J. Sci. Comput. **23**/6, (2002), p.2041-2054
- [3] E. Godlewski and P.-A. Raviart, *Numerical Approximation of Hyperbolic Systems of Conservation Laws*, Springer, New York (1996)

- 
- [4] E. Hairer, S. P. Norsett, and G. Wanner, Solving Ordinary Differential Equations, Volume I. Nonstiff Problems, Springer Series in Comput. Math. **8**, 2nd ed. Springer, Berlin (1993)
- [5] E. Hairer and G. Wanner, Solving Ordinary Differential Equations, Volume II. Stiff and Differential-Algebraic Problems, Springer Series in Comput. Math. **14**, 2nd ed. Springer, Berlin (1996)
- [6] P. J. van der Houwen and B. P. Sommeijer, *On the internal stability of explicit  $m$ -stage Runge-Kutta methods for large  $m$ -values*, Z. Angew. Math. Mech. **60**, (1980) p.479-485
- [7] W. Hundsdorfer and J. G. Verwer, Numerical Solution of Time-Dependent Advection-Diffusion-Reaction Equations, Springer Series in Computational Mathematics, Vol. 33, Springer, Berlin (2003)
- [8] H.-O. Kreiss and H. Ulmer-Busenhart, Time-dependant Partial Differential Equations and Their Numerical Solution, Birkhäuser, Basel (2001)
- [9] R. Jeltsch and O. Nevanlinna, *Largest Disk of Stability of Explicit Runge-Kutta Methods*, BIT **18**, (1978) p.500-502
- [10] R. Jeltsch and O. Nevanlinna, *Stability of Explicit Time Discretizations for Solving Initial Value Problems*, Numer. Math. **37**, (1981) p.61-91
- [11] V. I. Lebedev, *How to Solve Stiff Systems of Differential Equations by Explicit Methods*, in Numerical Methods and Applications, ed. by G. I. Marchuk, p.45-80, CRC Press (1994)
- [12] V. I. Lebedev and A. A. Medovikov, *An explicit method of the second order of accuracy for solving stiff systems of ordinary differential equations*, Russian Izv. Vyssh. Uchebn. Zaved. Mat. **9**, (1998) p.55-63
- [13] R. J. LeVeque, Finite Volume Methods for Hyperbolic Problems, Cambridge University Press, Cambridge (2002)
- [14] A. A. Medovikov, *High Order Explicit Methods for Parabolic Equations*, BIT **38**, (1998) p.372-390
- [15] Nowak, U. and Weimann, L.: *A Family of Newton Codes for Systems of Highly Nonlinear Equations - Algorithms, Implementation, Applications*, Zuse Institute Berlin, technical report TR 90-10, (1990), code available at [www.zib.de](http://www.zib.de)
- [16] B. Owren and K. Seip, *Some Stability Results for Explicit Runge-Kutta Methods*, BIT **30**, (1990), p.700-706
- [17] B. P. Sommeijer, L. F. Shampine, and J. G. Verwer, *RKC: an explicit solver for parabolic PDEs*, J. Comput. Appl. Math. **88**, (1998) p.316-326
- [18] M. Torrilhon, Explicit method for advection-diffusion equations, Example Implementation in C, code available online at [www.pacm.princeton.edu/~mtorrih/ExplCode](http://www.pacm.princeton.edu/~mtorrih/ExplCode), (2006)
- [19] J. G. Verwer, *Explicit Runge-Kutta methods for parabolic partial differential equations*, Appl. Num. Math. **22**, (1996) p.359-379
- [20] J. G. Verwer, B. P. Sommeijer and W. Hundsdorfer, *RKC time-stepping for advection-diffusion-reaction problems*, J. Comput. Phys. **201**, (2004), p. 61-79
- [21] P. Wesseling, Principles of Computational Fluid Dynamics, Springer Series in Computational Mathematics, Vol. 29, Springer, Berlin (2001)